

Iron-Catalyzed Direct Suzuki–Miyaura Reaction: Theoretical and Experimental Studies on the Mechanism and the Regioselectivity

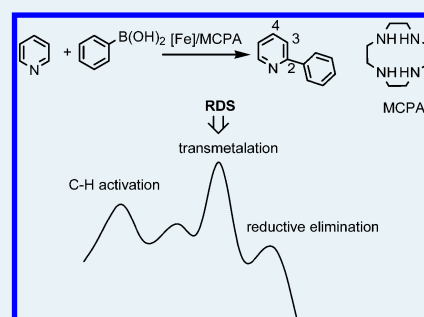
Liang Dong, Jun Wen, Song Qin, Na Yang, Huaqing Yang, Zhishan Su, Xiaoqi Yu, and Changwei Hu*

Key Laboratory of Green Chemistry and Technology, Ministry of Education, College of Chemistry, Sichuan University, Chengdu 610064, People's Republic of China

Supporting Information

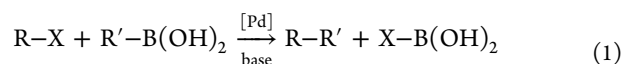
ABSTRACT: The mechanism of the Suzuki–Miyaura cross-coupling reaction between pyridine and phenylboronic acid catalyzed by the complex of iron salt combined with macrocyclic polyamine (iron–MCPA) was investigated theoretically and experimentally. It was found that the overall reaction includes three steps: C–H activation, transmetalation, and reductive elimination. The results indicate that the rate-determining step is the transmetalation step. The C–H activation of a different position on pyridine is the origin of the regioselectivity. The transmetalation step is the regio-determining step. Both the C–H activation and the transmetalation steps favor the regioselective formation of the ortho product. The oxoiron complex is predicted to be the active species theoretically and is confirmed by experiments. The calculations correctly reproduce the major product, 2-phenylpyridine, which is consistent with the experimental observation.

KEYWORDS: arylation, iron catalysis, mechanism, regioselectivity, DFT



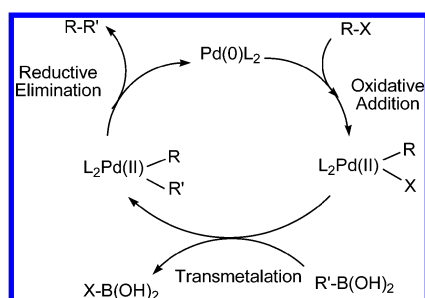
INTRODUCTION

The Suzuki–Miyaura cross-coupling reaction, in which organoboron compounds (mainly organoboronic acids) couple with organic halides (or triflates) in the presence of a Pd catalyst and a base, is one of the most efficient methods for the construction of C–C bonds (eq 1).^{1–6} Moreover, this reaction is extensively used in biaryl synthesis and medicinal and biological chemistry.^{7–12} Because of the commercial availability of organoboronic acids and its stability to heat, oxygen and water and the ease of handling and separation of boron-containing byproducts from the reaction mixtures, the Suzuki–Miyaura reaction has attracted much more attention.¹³



The traditionally accepted mechanism for the Suzuki–Miyaura cross-coupling reaction is depicted in Scheme 1.

Scheme 1. Traditionally Accepted Suzuki–Miyaura Cross-coupling Reaction Mechanism



Normally, the whole catalytic cycle includes three steps: (1) oxidative addition, (2) transmetalation, and (3) reductive elimination.^{14–17} The oxidative addition step is generally considered as the rate-determining step (RDS).

Although using a Pd catalyst to promote the Suzuki–Miyaura reaction is an ideal and green method, it also has many disadvantages, such as the requirements of directing the group on the substrate to promote selectivity and the relatively low yields of products. In recent years, cross-coupling reactions catalyzed by iron catalysts have been extensively explored because iron is a cost-effective, available, and environmentally benign catalyst capable of catalyzing effectively the cross-coupling reaction.^{18–22} Significant progress has been made in direct arylation using iron compounds.^{23–25}

Yu's group reported a novel method of direct arylation of unactivated arenes through iron catalysis.²⁶ Later, they developed a more convenient and easily handled iron-mediated Suzuki–Miyaura reaction for electron-rich and electron-deficient heteroarenes to avoid the requirement of large amounts of additives and low regioselectivity.²⁷ An appropriate combination of iron salt with macrocyclic polyamine (MCPA) was reported to effectively catalyze the Suzuki–Miyaura reaction. High regioselective (only ortho) products in moderate yields were obtained in the direct arylation of electron-rich heteroarene pyrrole catalyzed by iron(II)–MCPA (L1). Because it is an electron-deficient heteroarene, it is difficult to arylate pyridine through direct and selective C–H arylation.^{28–31} Yu's group reported that the

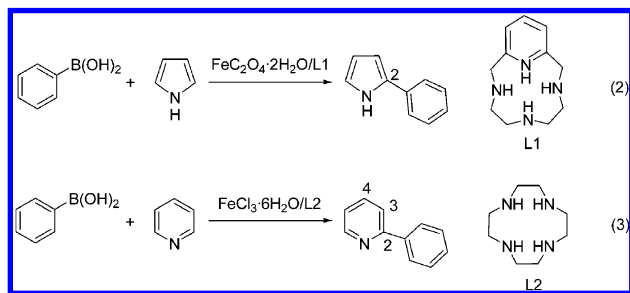
Received: January 14, 2012

Revised: May 16, 2012

Published: May 17, 2012

Suzuki–Miyaura reaction between pyridine and phenylboronic acid catalyzed by a iron(III)–MCPA (L2) complex could obtain 41% yield with 80:20 (o/(m + p)) regioselectivity (by GC/MS) in acetic acid (Scheme 2).

Scheme 2. Iron–MCPA Complex Catalyzed Direct Suzuki–Miyaura Reaction



Theoretical calculations concerning the Suzuki–Miyaura reaction catalyzed by Pd catalysts were recently carried out.^{32–40} Different stages, especially the specific transmetalation process, in the catalytic cycle were amply investigated. In contrast to Pd-catalyzed cross-coupling reactions, the theoretical calculation concerning the mechanism of the iron-catalyzed arylation is rare. Previously, we reported theoretical investigations concerning the iron(II)-catalyzed direct arylation of pyrrole.²⁷ The catalytic cycle was investigated roughly, and only a qualitative mechanistic depiction was presented for this reaction. Although a basic understanding of the cross-coupling catalytic cycle of the iron(II)-catalyzed direct arylation of pyrrole was obtained, the mechanism of the activation of the heterocycle C–H bond is still lacking. Furthermore, among the multiplicate heteroarenes, pyridine is of significant importance because of its simplest structure and important applications.^{28,41–43} However, the difficulty of the ortho arylation (C-2 position) of pyridine limited its applications.^{28–31} In an attempt to gain a better understanding of Suzuki–Miyaura reaction and to give guidance for promoting the reactivity and the regioselectivity of the arylation of pyridine, here, we present our theoretical and experimental results concerning the arylation reaction between pyridine and phenylboronic acid catalyzed by the iron(III)–L2 complex (Scheme 2, eq 3). Furthermore, we clarify the role of the solvent acetic acid in the reaction system in this paper.

THEORETICAL AND EXPERIMENTAL DETAILS

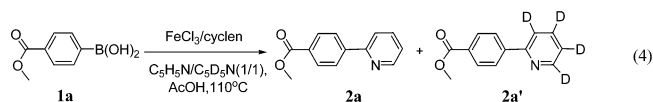
Computational Details. Previous investigations indicated that the B3LYP method can give reasonable structures and energies for iron-containing reactions.^{44–47} All the stationary points on the potential energy surface (PES) were optimized on the quartet and sextet spin states first using the hybrid density functional B3LYP^{48–50} method with the 6-31+G(d) basis set.^{51,52} Meanwhile, the test of stability of the density functional theory (DFT) wave function was passed. If an instability is found, the wave function is reoptimized, and the stability tests and reoptimizations are repeated until a stable wave function is found. To evaluate the reliability of the function theory levels, the reactants, the transmetalation transition states (TSs), and the products were reoptimized at the BPW91^{53,54}/6-31+G(d) and MPW1K⁵⁵/6-31+G(d) levels. The geometry optimizations have been observed to be relatively insensitive to the level of theory employed. Furthermore, we provided a suitable benchmark level of theory, including the solvent effect. Single-point energy

calculations (in acetic acid) were performed on the transmetalation TSs at the B3LYP/[6-311++G(d,p)], BPW91/[6-311++G(d,p)], and MPW1K/[6-311++G(d,p)] levels. The MPW1K method has been shown to provide highly accurate barrier heights.^{55,56} According to the experimental data, we considered the MPW1K/[6-311++G(d,p)] level would be suitable for studying the titled system.

Vibrational frequencies were obtained at the B3LYP/6-31+G(d) level, and the species were characterized as a minimum (no imaginary frequency) or a transition state (unique imaginary frequency). Intrinsic reaction coordinate (IRC) calculations^{57,58} were performed to further confirm that the optimized transition states correctly connect the relevant reactants and products. For evaluating the solvent effects, single-point MPW1K (PCM)/[6-311++G(d,p)] calculations were performed⁵⁹ on the optimized structures on the quartet and sextet spin states. Although the reaction was performed in acetic acid in the experiments, it is noteworthy that the highly excessive substrate pyridine was employed in the system (pyridine/acetic acid, 1:1).²⁷ Therefore the reaction was regarded as performed in mixed solvent (acetic acid/pyridine). The PCM calculations were performed in acetic acid ($\epsilon = 6.2$) and pyridine ($\epsilon = 12.3$), respectively, together with a UAHF radius. Unless otherwise stated, the relative energies used in the discussion are the total electronic energies in the PCM calculations at the MPW1K/[6-311++G(d,p)] level, including the zero-point energy correction at the B3LYP/6-31+G(d) level in the gas phase.

The chemical bonding properties were analyzed following the concepts developed in the theory of atoms-in-molecules (AIM2000), which provides a clear definition of a chemical bond by means of a topology analysis of $\rho(r)$.⁶⁰ To obtain further insight into the electroproperties along the reaction, natural bond orbital (NBO) analysis^{61,62} at the B3LYP/6-31+G(d) level was performed. KIE values were calculated on the basis of transition state theory at $p = 1$ atm and $T = 383.15$ K (110 °C).⁶³ All calculations were carried out with the Gaussian03 program.⁶⁴

General Procedure for ESI(+) HRMS Monitoring. A reflux tube equipped with a magnetic stirring bar was charged with phenylboronic acid (0.2 mmol, 1.0 equiv), $\text{FeCl}_3 \cdot 6\text{H}_2\text{O}$ (0.5 equiv), L2 (0.5 equiv), pyridine (1 mL), and acetic acid (1 mL). The reaction vessel was placed in a 110 °C oil bath. ESI-HRMS was used to monitor the reaction by sampling at different times. This reaction was studied at 15, 30, and 90 min. ESI-MS spectral data were recorded on a Finnigan LCQDECA mass spectrometer.



General Procedure for KIE Effect Determination (eq 4).

A reflux tube equipped with a magnetic stirring bar was charged with 4-(methoxycarbonyl)phenylboronic acid (**1a**, 0.2 mmol, 1.0 equiv), $\text{FeCl}_3 \cdot 6\text{H}_2\text{O}$ (0.5 equiv), L2 (0.5 equiv), equimolar pyridine and pyridine- d_5 (1 mL), and acetic acid (1 mL), and the reaction vessel was placed in a 110 °C oil bath. After stirring at this temperature for 6 h, the mixture was cooled to room temperature and diluted with ethyl acetate. The resulting solution was directly filtered through a pad of silica and concentrated in vacuo. The crude product was purified by column chromatography (Al_2O_3 , petroleum ether/ethyl acetate, 20:1). According to ^1H NMR data, the reaction gave 0.50:0.50

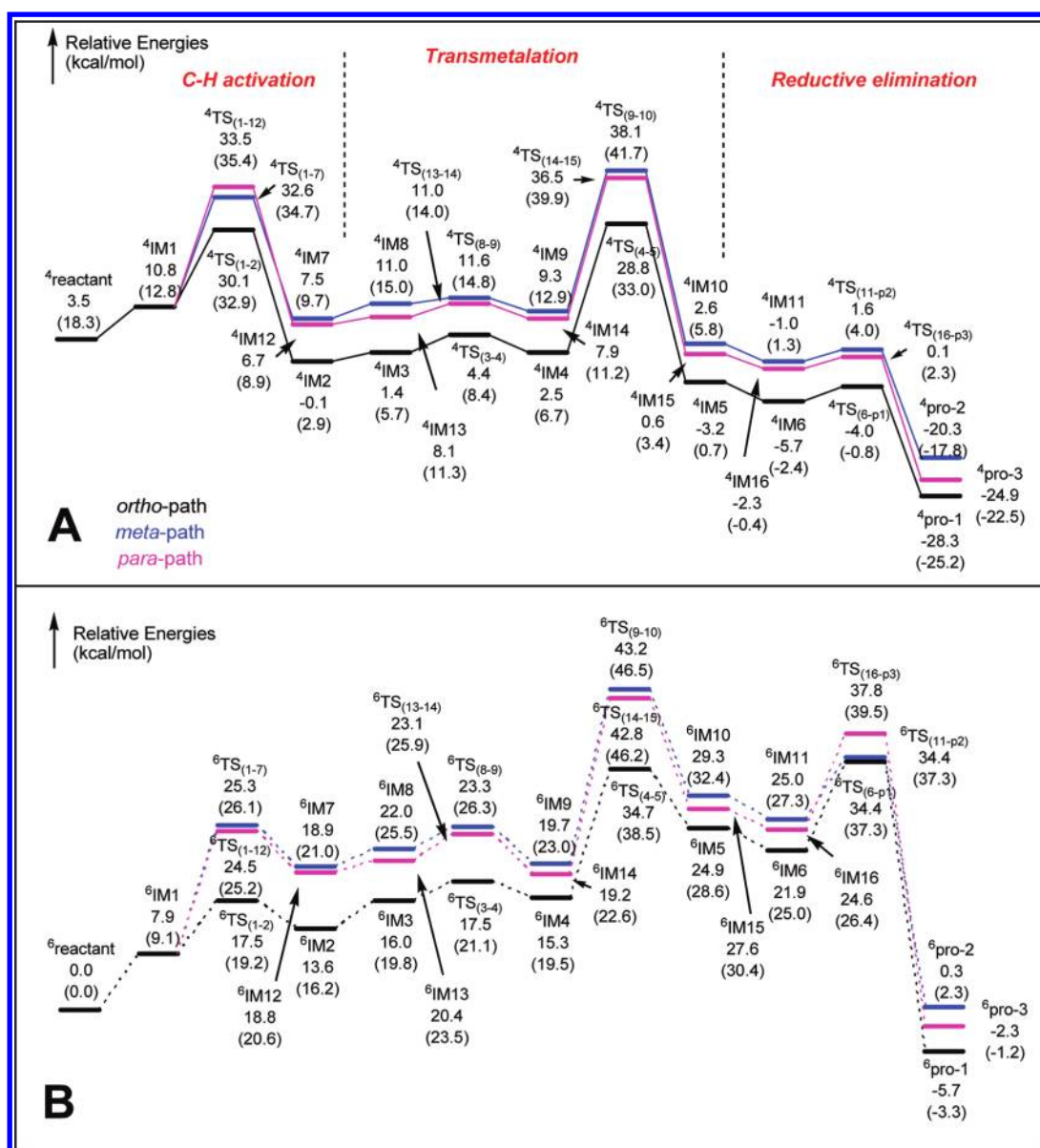


Figure 1. PCM energies (in kcal/mol) in acetic acid for various IMs and TSs involved in the iron–L2-catalyzed reaction. PCM energies (in kcal/mol) in pyridine are listed in parentheses. The species on the quartet PESs are presented in part A (solid curve), and the ones on the sextet PESs are presented in part B (dashed curve). (The black, blue, and red curves represent the paths along the arylation of pyridine at the ortho, meta, and para positions, respectively.).

ratios of **2a** and **2a'**, which indicated that the intermolecular isotope effect of k_H/k_D was 1.0. The ^1H NMR spectra were measured on a Bruker AM400 NMR spectrometer (400 MHz) with CDCl_3 as solvent and recorded in parts per million relative to the internal tetramethylsilane standard.

General Procedure for the Arylation of Pyridine in the Absence of Solvent. The arylation of pyridine in the absence of acetic acid was performed according to the literature procedure.²⁷ A reflux tube equipped with a magnetic stirring bar was charged with phenylboronic acid (0.2 mmol, 1.0 equiv), $\text{FeCl}_3 \cdot 6\text{H}_2\text{O}$ (0.5 equiv), L2 (0.5 equiv), and pyridine (1 mL), and the reaction vessel was placed in a 110 °C oil bath. After stirring at this temperature for 12 h, the mixture was cooled to room temperature. The yield and the ratio of regioisomers of the product were determined by GC/MS (Agilent, 6890-5973N) using *n*-dodecane as an internal standard.

RESULTS AND DISCUSSION

Theoretical Section. *The Oxoiron Species-Catalyzed Process.* In the present system, we continue the previous proposal²⁷ concerning the rare oxoiron^{63,65} complex as the most probable effective catalytic species in the reaction. The possibility of the formation of the oxoiron–L2 complex ($\text{FeO}^+-\text{L2}$) in this reaction system was studied theoretically, and through geometry optimization, $\text{FeO}^+-\text{L2}$ was identified as stable, as shown in Figure 2. Furthermore, $\text{FeO}^+-\text{L2}$ was observed by ESI-MS (see the Experimental Section).

Our calculations start from the simulation on the Suzuki–Miyaura reaction between pyridine and phenylboronic acid catalyzed by $\text{FeO}^+-\text{L2}$. Figure 1 shows the calculated PCM energy surfaces in acetic acid (or in pyridine) at the MPW1K/6-311++G(d,p) level on the sextet and quartet states. It is shown

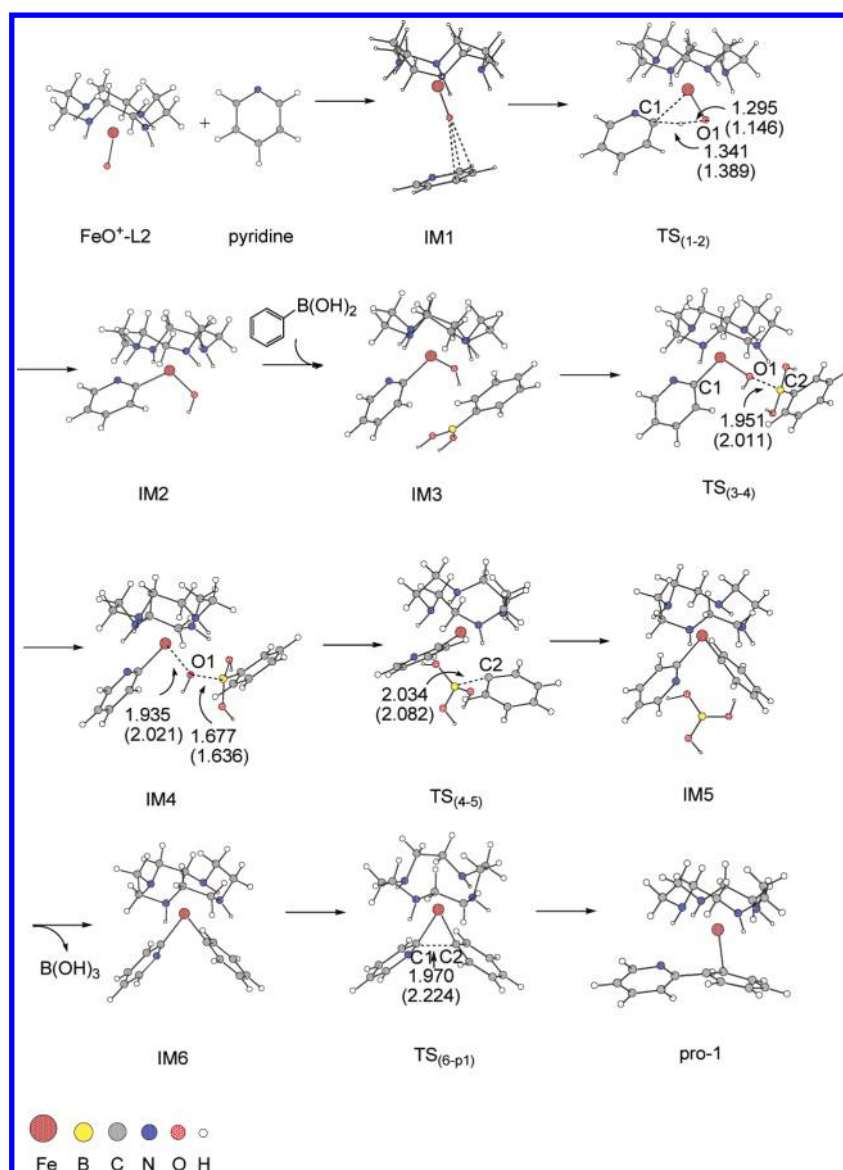


Figure 2. The optimized structures of the iron-L2-catalyzed direct ortho arylation of pyridine and phenylboronic acid. (Bond lengths of the optimized structures on the quartet are presented, and the ones on the sextet are listed in parentheses, bond lengths in Å.).

that the variation trend in pyridine is the same as that in acetic acid.

The calculations indicate that the overall reaction is composed of three steps: C–H activation, transmetalation, and reductive elimination. The arylation of pyridine occurs at the ortho, meta, and para positions; in addition, the corresponding structures on the quartet and the sextet surface are optimized. Therefore, six paths similar in mechanism and energies are obtained. Because the ortho path is the most kinetically and thermodynamically favored in acetic acid (or in pyridine), it was chosen to illustrate the mechanism of the direct Suzuki–Miyaura reaction. The optimized structures along the ortho path are given in Figure 2.

As shown in Figure 2, the reaction starts with an electrophilic attack of the oxoiron–L2 toward the ortho position C atom of the pyridine ring with the assistance of the N atom. Subsequently, the binary complex forms, followed by a hydrogen migration from the ortho position C atom of pyridine to the oxoiron–L2. The tertiary complex consisting of iron, pyridine, and L2 ligand generates after the C–H activation. Next, phenylboronic acid enters the catalytic cycle. The transmetalation occurs between

the tertiary complex and phenylboronic acid, with the formation of boric acid. Finally, the reductive elimination generates the product complex. The specific bond lengths involved in the TSs on the quartet (sextet) state are also presented in Figure 2. It is worth noting that the bond lengths of Fe–O1 and O1–B in ⁴IM4 are 1.935 and 1.667 Å (2.021 and 1.636 Å in ⁶IM4); however, the bond lengths of Fe–O1 and O1–B are 1.891 and 1.951 Å in ⁴TS_(3–4) (1.936 and 2.011 Å in ⁶TS_(3–4)) and 2.197 and 1.455 Å in ⁴TS_(4–5) (2.134 and 1.443 Å in ⁶TS_(4–5)). The results indicate that the interaction between the Fe and O1 atoms is weaker than normal bonding. The interaction between the O1 and B atoms is similar to that between the Fe and O1 atoms. Thus, IM4 would be better viewed as an ionic pair with organoboronate than an intermediate.

As shown in Figure 1, it is found that the minimum energy PES is not one of the two PESs. The sextet entrance channel is lower in energy than the quartet one, and after the C–H activation, the rest of the local minima of the quartet PES lie lower than the corresponding sextets. This result clearly indicates that both PESs must cross each other, and a minimum energy crossing

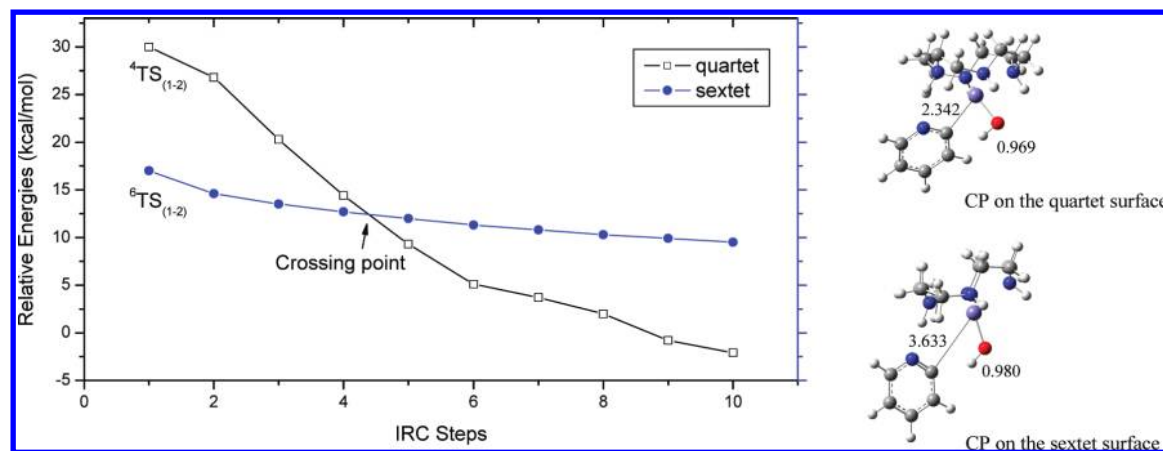


Figure 3. IRC analysis for the C–H activation TSs (${}^4\text{TS}_{(1-2)}$ and ${}^6\text{TS}_{(1-2)}$) and the geometries of the approximate crossing point.

point may exist. To check the possibility of the quartet and sextet intersections and to locate the crossing point, IRC analysis was carried out for the C–H activation TSs (${}^4\text{TS}_{(1-2)}$ and ${}^6\text{TS}_{(1-2)}$). Figure 3 presents the evolutions of the relative energies as the reaction proceeds along the intrinsic reaction coordinate. From Figure 3, it can be seen that the relative energies of ${}^4\text{TS}_{(1-2)}$ decrease dramatically, and the relative energies of ${}^6\text{TS}_{(1-2)}$ decrease gently along the intrinsic reaction coordinate. The approximate crossing point between the two surfaces occurs at IRC = 4 bohr^{1/2}, and the geometries of the approximate crossing point are shown in Figure 3. According to the IRC analysis, it is clear that the crossing of potential energy surfaces of quartet and sextet spin states is involved in the reaction process. For the ortho path, the minimum energy reaction pathway should be ${}^6\text{FeO}^+ - \text{L2} + \text{pyridine} \rightarrow {}^6\text{IM1} \rightarrow {}^6\text{TS}_{(1-2)} \rightarrow {}^4\text{IM2} + \text{PhB}(\text{OH})_2 \rightarrow {}^4\text{IM3} \rightarrow {}^4\text{TS}_{(3-4)} \rightarrow {}^4\text{IM4} \rightarrow {}^4\text{TS}_{(4-5)} \rightarrow {}^4\text{IM5} - \text{B}(\text{OH})_3 \rightarrow {}^4\text{IM6} \rightarrow {}^4\text{TS}_{(6-p1)} \rightarrow {}^4\text{pro-1}$.

The relative energy of ${}^4\text{TS}_{(4-5)}$ is calculated to be 28.8 kcal/mol in acetic acid (or 33.0 kcal/mol in pyridine). This result indicates that the transmetalation step is the RDS in the reaction. The calculated relative energy is a little high, corresponding to the difficulty of the arylation of pyridine, which implies that the reaction needs a certain temperature and reaction time.

Since our calculations indicate that the transmetalation step is the RDS for the reaction, the result is clearly incompatible with the traditional mechanism^{66–69} for this type of arylation processes. In those transition metal-catalyzed reactions (for example, Pd complex-catalyzed reactions), the transmetalation takes place with a four-membered TS with relatively low energies, and the oxidative addition has been often proposed as the RDS in the catalytic cycle. However, it is known that to take place, the traditional Suzuki–Miyaura reaction requires the presence of a base. Braga et al. reported the DFT calculations of the palladium catalyzed Suzuki–Miyaura reaction^{35,40} and found that the Suzuki–Miyaura reaction proceeded quite smoothly in the presence of a base (OH^-), but when the reaction proceeded in the absence of base, the energy barrier of the transmetalation step is rather high compared with the separated reactants. In the present system, because acetic acid is the solvent, there is no strong base (pyridine is the substrate, and the amount is less), and the reaction is in an acidic system. Thus, this might explain why the result is incompatible with the traditional mechanism, and the transmetalation is the RDS in the present system.

Since the presence of kinetic isotope effects (KIE) can provide valuable information about the RDS in chemical processes,^{70–73}

we calculated the KIE values for the C–H activation step via ${}^6\text{TS}_{(1-2)}$ and the transmetalation step via ${}^4\text{TS}_{(4-5)}$ in acetic acid (or pyridine) at $p = 1$ atm and $T = 383.15$ K for the most kinetically favored ortho path. If the RDS were the C–H activation, the KIE ($k_{\text{H}}/k_{\text{D}}$) value should be 7.7 in acetic acid (or 5.9 in pyridine). Considering transmetalation as the RDS, the KIE value is computed to be 0.8 in acetic acid (or 0.7 in pyridine). Since the isotope effect of $k_{\text{H}}/k_{\text{D}} = 1.0$ was observed in the experiments (see Experimental Section), it is revealed by experiment that the actual reaction rate is irrelevant to the C–H activation step. Thus, it is reasonable for us to believe that the transmetalation step is the RDS.

The Recovery of the Catalytically Active Species.

During the oxoiron species-catalyzed process, Fe(III) of the oxoiron species is reduced to Fe(I). After the generation of the product and the expulsion of the Fe^+ species, Fe(I) is oxidized by an oxygen to Fe(III). The recovery of the FeO^+ species has been accomplished (eq 5).



We investigated the possible reaction pathways on the singlet, quintet, and nonet spin potential surfaces from $2\text{L2}-\text{Fe}^+ + \text{O}_2$. Since the calculated relative energies on the singlet and quintet states are much higher than those on the nonet state, we presented the results of only the most feasible nonet spin state.

Figure 4 shows the calculated PCM energy surfaces of the oxidation process from Fe(I) to Fe(III) by O_2 in acetic acid (or in pyridine) at the MPW1K/6-311++G(d,p) level on the nonet state. The variation trend in pyridine is the same as that in acetic acid.

As shown in Figure 4, two $\text{Fe}(\text{I})^+ - \text{L2}$ first coordinate to one oxygen, generating the complex ${}^9\text{IM1}_{\text{Fe}(\text{I})\text{L2}-\text{O}_2}$. Next, the cleavage of the O–O bond occurs via ${}^9\text{TS1}_{\text{Fe}(\text{I})\text{L2}-\text{O}_2}$. As shown in Figure 4, the resulting $\text{L2}-\text{FeO}^+$ species on the sextet is more stable relative to the quartet $\text{L2}-\text{FeO}^+$. The minimum energy reaction pathway should be ${}^9\text{IM1}_{\text{Fe}(\text{I})\text{L2}-\text{O}_2} + {}^9\text{TS1}_{\text{Fe}(\text{I})\text{L2}-\text{O}_2} \rightarrow {}^6\text{Fe}(\text{III})\text{O}-\text{L2}$.

The Role of the Solvent. At the end of this section, we wish to mention the solvent effects on the energy changes. As mentioned previously,²⁷ the iron–L2 catalyzed Suzuki–Miyaura reaction could give 41% yield under the condition of pyridine/acetic acid = 1:1. Although the excessive pyridine can be regarded as another solvent, the more crucial role of pyridine is the substrate as compared with acetic acid. Therefore, PCM calculations were performed in both acetic acid and pyridine to clarify the role of

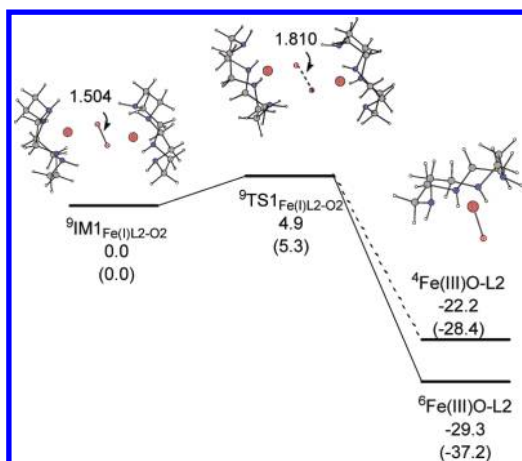


Figure 4. PCM energies (in kcal/mol) in acetic acid for the optimized structures involved in the recovery process. PCM energies (in kcal/mol) in pyridine are listed in parentheses. (The solid curve represents the sextet surface, and the dashed one represents the quartet surface.)

acetic acid via comparison with pyridine. The PCM calculations clearly show that the solvent effects do not alter the positions of the minima but reduce the relative energies of PES. As shown in Figure 1, the energies of PES in acetic acid are much lower than those in pyridine. This result indicates that the reaction might be thermodynamically favored in acetic acid.

Furthermore, because acetic acid is the solvent, we also considered the possibility of the protonation of pyridine, but the calculations failed to locate the corresponding structures along the path of the pyridinium cation as the substrate.

The Origin of the Regioselectivity. As an important factor when considering the application of a methodology in synthesis, regioselectivity issues in direct arylation have been studied frequently.^{44,73,74} After the mechanism of the direct Suzuki–Miyaura reaction is obtained, it is very interesting to investigate the regioselectivity. Yu's group²⁷ reported that the direct Suzuki–Miyaura reaction catalyzed by the iron–L2 could obtain 80:20 (o/(m + p)) regioselectivity (Scheme 2, eq 3). On the basis of the experimental data, the Suzuki–Miyaura reaction between pyridine and phenylboronic acid catalyzed by iron–L2 was chosen to investigate the regioselectivity of the products.

As previously mentioned, the reaction is initiated by the attack of the active species FeO^+ toward one C atom next to the N atom on the pyridine ring. Next, the cleavage of C–H bond occurs on the attacked C atom, and the H atom migrates from pyridine to FeO^+ . It is obvious that during this step, the C–H activation of a different position of pyridine leads to the formation of the regioisomeric cross-coupling products. In other words, the C–H activation is the origin of the regioselectivity.

Since the C–H activation of pyridine could occur at the ortho, meta, and para positions (C-2, C-3, and C-4 positions) on the pyridine, three distinct C–H activation TSs ($\text{TS}_{(1-2)}$, $\text{TS}_{(1-7)}$ and $\text{TS}_{(1-12)}$) were obtained. The attacked position of the FeO^+ toward the C atom on the pyridine ring and the optimized structures of the C–H activation TSs along different paths are given in Figure 5.

The C–H activation transition states, as shown in Figure 5, are responsible for the C–H bond dissociation of the C-2, C-3, or C-4 site of pyridine ring and the O–H bond formation. They connect the oxoiron–MCPA–heterocycle complex and the hydroxoiron–MCPA–heterocycle intermediates. As shown in Figure 1, the three lowest-energy TSs obtained by the different

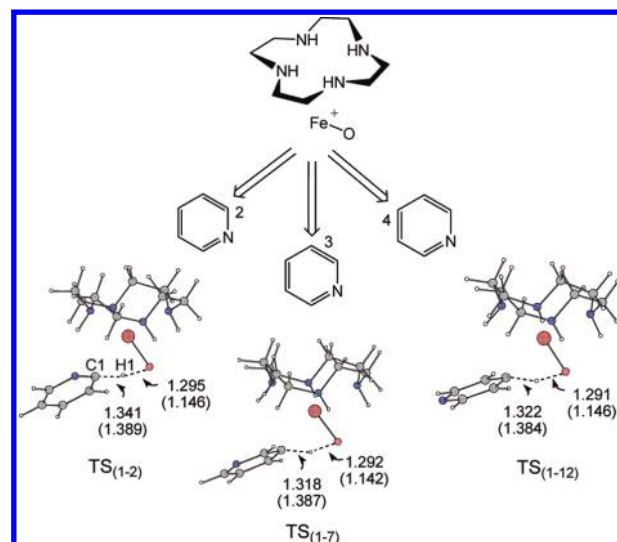


Figure 5. The attack position of the FeO^+ toward the C atom on the pyridine ring and the optimized structures of the C–H activation TSs along different paths. (Bond lengths of the optimized structures on the quartet are presented, and the ones on the sextet are listed in parentheses, bond lengths in Å.)

attack positions of the FeO^+ species to the C atom are ${}^6\text{TS}_{(1-2)}$, ${}^6\text{TS}_{(1-7)}$, and ${}^6\text{TS}_{(1-12)}$, respectively. The calculated relative energies of ${}^6\text{TS}_{(1-2)}$ are 17.5 kcal/mol in acetic acid (or 19.2 kcal/mol in pyridine), kinetically favored by more than 7 kcal/mol in acetic acid (or 6 kcal/mol in pyridine) as compared with ${}^6\text{TS}_{(1-7)}$ and ${}^6\text{TS}_{(1-12)}$. The results indicate that the attack of the FeO^+ species to the C atom would prefer to occur at the C-2 site of the pyridine ring.

Herein, the different attacked position of the FeO^+ species to C atom on the pyridine ring leads to the regioselective formation of the products. To understand the details of electronic evolution and clarify the reason producing the regioselectivity from more micro aspects, IRC analysis was carried out for the kinetically favored ${}^6\text{TS}_{(1-2)}$ transition structure. Figure 6 presents the

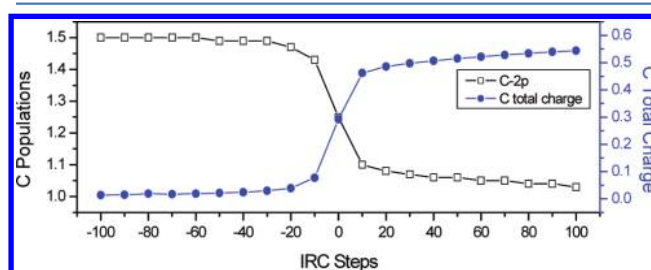


Figure 6. The electronic populations and the distribution of the total charge on C1 atom along IRC.

evolutions of the electronic populations and the total charge on C1 atom as the reaction proceeds along the intrinsic reaction coordinate (see the Supporting Information for IRC plots).

Along the structural evolution, a considerable amount of charge is reorganized among the C1, H1, and O atoms. NBO analysis illustrates that, from ${}^6\text{IM1}$ to ${}^6\text{IM2}$, accompanied by the cleavage of C1–H1 bond and the formation of H1–O bond, the electronic population on the 2p orbital of C1 atom decreases from 1.50 to 1.03. For the total charge distribution of the C1 atom, from ${}^6\text{IM1}$ to ${}^6\text{IM2}$, the charge on the C1 atom increases gradually from 0.011e to 0.550e. Meanwhile, the charge on the O

atom changes from $0.015e$ at $\text{IRC} = -100 \text{ bohr}^{1/2}$ to $-0.441e$ at $\text{IRC} = 100 \text{ bohr}^{1/2}$. This result indicates that the charge on the O atom transfers to the C1 atom during the formation of ${}^6\text{IM2}$.

Consequently, after the FeO^+ species attacks pyridine, the charge transfers from the O atom to the C1 atom on pyridine. The increasing charge on the C1 atom makes the C atom become more nucleophilic and the interaction between pyridine and FeO^+ greater. This might be responsible for the favored transition state ${}^6\text{TS}_{(1-2)}$ in C–H activation TS.

The Determination of the Regioselectivity. Knowing that the C–H activation of different positions on pyridine leads to the regioselective formation of the products, we turned our attention to the RDS: transmetalation. The RDS determines the ratio of the regioisomers; thus, the transmetalation step is the regio-determining step.

The optimized structures of the three regioisomeric TSs in transmetalation step are provided in Figure 7. The PCM energies of the optimized structures in acetic acid (or in pyridine) at the MPW1K/6-311++G(d,p) level are also given in Figure 7.

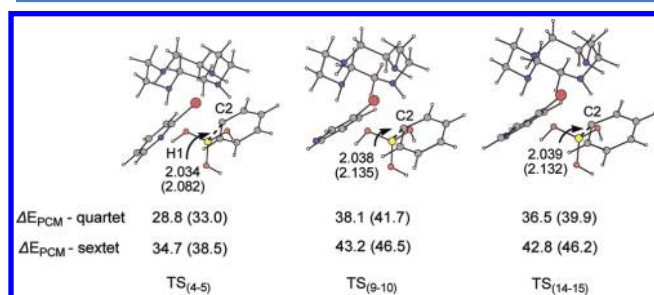


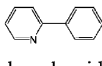
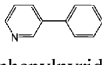
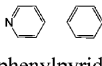
Figure 7. The optimized structures of the transmetalation TSs along different paths. (Bond lengths of the optimized structures on the quartet are presented and the ones on the sextet are listed in parentheses.) PCM energies (in kcal/mol) in acetic acid for various TSs. PCM energies (in kcal/mol) in pyridine are listed in parentheses.

As shown in Figure 7, the calculations indicate that the transition states on the quartet PES are kinetically favored, as compared with those on the sextet. The structures of the products and the PCM energies of the energetically favored quartet TSs at the MPW1K/6-311++G(d,p) level are summarized in Table 1.

It is observed that ${}^4\text{TS}_{(4-5)}$ is the lowest-energy TS corresponding to the product 2-phenylpyridine by comparing the calculated PCM energies in acetic acid of the three regioisomeric TSs, as shown in Table 1. The results show that the ortho path is preferable over the meta and para paths, and the 2-phenylpyridine might be the major product in the reaction. This is consistent with the experimental observation. Because of the electron-withdrawing effect of the N atom on the pyridine ring, the electron deficiency of the ortho position C atom next to the N atom might be responsible for the easier C–H arylation of the C-2 site. However, as shown in Table 1, the calculated energies of ${}^4\text{TS}_{(4-5)}$ in acetic acid are preferred by 9.3 and 7.7 kcal/mol as compared with ${}^4\text{TS}_{(9-10)}$ and ${}^4\text{TS}_{(14-15)}$, respectively. On the basis of the calculated energy differences among the three regioisomeric TSs, the predicted regioselectivities are overestimated as compared with the experiment results.

From Figure 7, it should be noted that in ${}^4\text{TS}_{(4-5)}$ along the ortho path, the N atom of pyridine is closed to the H1 atom in $\text{B}(\text{OH})_3$, and the $\text{N}\cdots\text{H1}$ distance is only 1.924 Å. AIM analysis indicates that the calculated Laplacian $L(r)$ at the bond critical point between N and H1 in ${}^4\text{TS}_{(4-5)}$ is -0.026 au , showing that

Table 1. Relative Energies (in kcal/mol) of Transmetalation TSs

Structures	Products	ΔE_{PCM}^a	ΔE_{PCM}^b
${}^4\text{TS}_{(4-5)}$	 2-phenylpyridine	28.8	33.0
${}^4\text{TS}_{(9-10)}$	 3-phenylpyridine	38.1	41.7
${}^4\text{TS}_{(14-15)}$	 4-phenylpyridine	36.5	39.9

^aSingle-point MPW1K (PCM, acetic acid)/[6-311++G(d,p)] calculations.
^bSingle-point MPW1K (PCM, pyridine)/[6-311++G(d,p)] calculations.

^aSingle-point MPW1K (PCM, acetic acid)/[6-311++G(d,p)] calculations. ^bSingle-point MPW1K (PCM, pyridine)/[6-311++G(d,p)] calculations.

the hydrogen bonding interaction exists between N and H1. As compared with ${}^4\text{TS}_{(4-5)}$ shown in Figure 7, hydrogen bonding interaction between N and H1 likely does not exist in ${}^4\text{TS}_{(9-10)}$ and ${}^4\text{TS}_{(14-15)}$, which is suggested by the relative positions between the N atom in pyridine and the H1 atom in $\text{B}(\text{OH})_3$ and the corresponding $\text{N}\cdots\text{H1}$ distances of 3.842 and 4.928 Å in ${}^4\text{TS}_{(9-10)}$ and ${}^4\text{TS}_{(14-15)}$, respectively. In addition, there is no significant difference in structural distortion in the three structures of the transmetalation TSs. Since the hydrogen bonding could stabilize the conformer, thereby facilitating the reaction,^{75,76} the relative energies of ${}^4\text{TS}_{(4-5)}$ in acetic acid are much lower than those of ${}^4\text{TS}_{(9-10)}$ and ${}^4\text{TS}_{(14-15)}$.

The hydrogen bonding interaction might be responsible for underestimation of the activation barrier of the ortho-substituted transmetalation TS. Our results qualitatively show that the ortho path is preferable to the meta and para paths. On the other hand, such great energy differences between ${}^4\text{TS}_{(4-5)}$ and the other two regioisomeric TSs obtained in acetic acid might also suggest that acetic acid is favorable for ensuring the regioselectivity in the reaction system. It is noted that PCM calculations in pyridine also lead to the major product 2-phenylpyridine.

These calculations indicate that the regioselectivity of this reaction is affected by the C–H activation and the transmetalation steps together, and both steps favor the regioselective formation of the ortho product.

EXPERIMENTAL SECTION

The Confirmation of the Oxoiron Species by ESI-MS. A cluster of peaks at $m/z = 554\text{--}557$ was observed by ESI-MS, which implied that the predicted catalytically active species $\text{FeO}^+\text{--L2}$ existed in the system (details in Supporting Information, Figure S1). It is found that the structure of $\text{FeO}^+\text{--L2}$ is similar to that of $\text{FeO}^+\text{--L1}$ proposed previously.²⁷

The Observation of the Intermediates by ESI-MS. During the entire catalytic process, we predicted several key intermediates. Among these intermediates, the catalyst–product complex, named as (pro.), is the most stable one on the PES. Since the mass spectra observed by ESI-MS has become a powerful tool in the identification of organic and organometallic reaction intermediates,^{77–80} we utilized ESI-MS to monitor the possible intermediates. A new cluster of peaks at $m/z = 788\text{--}791$ was observed at 30 min by ESI-MS (details in Supporting

Information, Figure S1-B). This result indicates that the computed structure of the catalyst–product complex might exist in the system. Although ESI-MS investigation does not provide detailed structural information about the intermediates, the observed mass spectra corresponding to the key intermediates in the proposed mechanism could validate the suggested mechanism from another aspect.

The Confirmation of the RDS. To confirm our predictions concerning the RDS in the present system, here, a substantial deuterium isotope effect was determined to confirm our predictions concerning the RDS in the present system. An intramolecular isotope effect of $k_{\text{H}}/k_{\text{D}} = 1.0$ at 110 °C (details in Supporting Information, Figure S2) has been determined, which suggests that the C–H bond dissociation of the pyridine ring in the course of pyridine arylation is not the RDS. Combined with the predicted KIE values for the C–H activation step and the transmetalation step (see Theoretical Section), it is concluded that the transmetalation step is the RDS. In summary, both theoretical and experimental evidence demonstrate that the transmetalation step is the RDS in the present system.

The Role of the Solvent. To further investigate the effects of acetic acid, we experimentally performed the Suzuki–Miyaura reaction catalyzed by iron–L2 in the absence of acetic acid, and only 24.5% yield was obtained with 50:50 (o/(m + p)) regioselectivity by GC/MS. The low yield and regioselectivity obtained in the absence of acetic acid confirm our prediction that acetic acid is favorable for this reaction. Hence, both theoretical and experimental results demonstrate that acetic acid might facilitate the reaction compared with pyridine. Therefore, the positive impacts of acetic acid on the reactivity and regioselectivity for the Suzuki–Miyaura reaction might be the reasons why acetic acid was selected as the solvent in experiments.

CONCLUSIONS

The mechanism and the regioselectivity of the Suzuki–Miyaura reaction catalyzed by iron–L2 have been investigated theoretically and experimentally. The effects of the solvent acetic acid on the mechanism and the regioselectivity are also interpreted. The major conclusions are listed as the following:

The catalytic cycle may include three steps: C–H activation, transmetalation, and reductive elimination. The RDS is the transmetalation step.

The C–H activation of different positions on pyridine is the origin of the regioselectivity. The transmetalation is the regio-determining step. The regioselectivity is affected by the C–H activation and the transmetalation steps together. After the FeO^+ species attacks pyridine, the charge transfers from the O atom of FeO^+ to the C-2 atom of pyridine. The increasing charge on the C atom makes the C atom become more nucleophilic and the interaction between pyridine and FeO^+ greater. Therefore, the arylation of pyridine favors the regioselective formation of the ortho product. The major product 2-phenylpyridine reproduced theoretically is consistent with the experimental observation.

The mass spectra observed by ESI-MS experiments support the existence of the theoretically predicted catalytically active species FeO^+ and the intermediate of the catalyst–product complex.

Acetic acid is favorable for this reaction system for both the reactivity and the regioselectivity.

ASSOCIATED CONTENT

Supporting Information

Computational methods, optimized geometries, and the calculated energies. This material is available free of charge via the Internet at <http://pubs.acs.org>.

AUTHOR INFORMATION

Corresponding Author

*Phone: +86-28-85411105. Fax: +86-28-85411105. E-mail: chwehu@mail.sc.cninfo.net, gchem@scu.edu.cn.

Notes

The authors declare no competing financial interest.

ACKNOWLEDGMENTS

The authors are grateful for financial support provided by NNSF (Nos. 21021001, 20732003, and 20772085) and PCSIRT (No. IRT0846) of China and the Specialized Research Fund for the Doctoral Program of Higher Education (No. 200806101007).

REFERENCES

- (1) Miyaura, N.; Yanagi, T.; Suzuki, A. *Synth. Commun.* **1981**, *11*, 513–519.
- (2) Miyaura, N.; Suzuki, A. *Chem. Rev.* **1995**, *95*, 2457–2483.
- (3) Martin, R.; Buchwald, S. L. *Acc. Chem. Res.* **2008**, *41*, 1461–1473.
- (4) Yu, D.; Shi, Z. *Angew. Chem., Int. Ed.* **2011**, *50*, 7097–7100.
- (5) Shi, Z.; Li, B.; Wan, X.; Cheng, J.; Fang, Z.; Cao, B.; Qin, C.; Wang, Y. *Angew. Chem., Int. Ed.* **2007**, *46*, 5554–5558.
- (6) Yang, S.; Sun, C.; Fang, Z.; Li, B.; Li, Y.; Shi, Z. *Angew. Chem., Int. Ed.* **2008**, *47*, 1473–1476.
- (7) Selander, N.; Szabó, K. J. *Chem. Rev.* **2010**, *111*, 2048–2076.
- (8) Rosen, B. M.; Quasdorf, K. W.; Wilson, D. A.; Zhang, N.; Resmerita, A.; Garg, N. K.; Percec, V. *Chem. Rev.* **2010**, *111*, 1346–1416.
- (9) Schneider, F.; Stolle, A.; Ondruschka, B.; Hopf, H. *Org. Process Res. Dev.* **2009**, *13*, 44–48.
- (10) Omumi, A.; Beach, D. G.; Baker, M.; Gabryelski, W.; Manderville, R. A. *J. Am. Chem. Soc.* **2011**, *133*, 42–50.
- (11) Zhang, S.; Wang, Z.; Xu, M.; Lin, G. *Org. Lett.* **2010**, *12*, 5546–5549.
- (12) Sun, C.; Liu, N.; Li, B.; Yu, D.; Wang, Y.; Shi, Z. *Org. Lett.* **2010**, *12*, 184–187.
- (13) Hall, D. G. *Boronic Acids*; Wiley-VCH: Weinheim, 2005.
- (14) Lafrance, M.; Fagnou, K. *J. Am. Chem. Soc.* **2006**, *128*, 16496–16497.
- (15) Goossen, L. J.; Koley, D.; Hermann, H. L.; Thiel, W. *Organometallics* **2005**, *24*, 2398–2410.
- (16) *Metal Catalyzed Cross-Coupling Reactions*; Diederich, F., de Meijere, A., Eds.; John Wiley & Sons: New York, 2004.
- (17) Miyaura, N. *Top. Curr. Chem.* **2002**, *219*, 11–59.
- (18) Sun, C.; Li, B.; Shi, Z. *Chem. Rev.* **2010**, *111*, 1293–1314.
- (19) Sherry, B. D.; Fürstner, A. *Acc. Chem. Res.* **2008**, *41*, 1500–1511.
- (20) Bolm, C.; Legros, J.; Paih, J. L.; Zani, L. *Chem. Rev.* **2004**, *104*, 6217–6254.
- (21) Li, Y.; Li, B.; Lu, X.; Lin, S.; Shi, Z. *Angew. Chem., Int. Ed.* **2009**, *48*, 3817–3820.
- (22) *Iron Catalysis in Organic Chemistry: Reactions and Applications*; Plietker, B., Ed.; Wiley-VCH: Weinheim, 2008.
- (23) Vallée, F.; Mousseau, J. J.; Charette, A. B. *J. Am. Chem. Soc.* **2010**, *132*, 1514–1516.
- (24) Sarhan, A. A. O.; Bolm, C. *Chem. Soc. Rev.* **2009**, *38*, 2730–2744.
- (25) Correa, A.; Mancheño, O. G.; Bolm, C. *Chem. Soc. Rev.* **2008**, *37*, 1108–1117.
- (26) Wen, J.; Zhang, J.; Chen, S.; Li, J.; Yu, X. *Angew. Chem., Int. Ed.* **2008**, *47*, 8897–8900.
- (27) Wen, J.; Qin, S.; Ma, L.; Dong, L.; Zhang, J.; Liu, S.; Duan, Y.; Chen, S.; Hu, C.; Yu, X. *Org. Lett.* **2010**, *12*, 2694–2697.

- (28) Xu, J.; Cheng, G.; Su, D.; Liu, Y.; Wang, X.; Hu, Y. *Chem.—Eur. J.* **2009**, *15*, 13105–13110.
- (29) Esteruelas, M. A.; Forcén, E.; Oliván, M.; Oñate, E. *Organometallics* **2008**, *27*, 6188–6192.
- (30) Harrison, D. P.; Sabat, M.; Myers, W. H.; Harman, W. D. *J. Am. Chem. Soc.* **2010**, *132*, 17282–17295.
- (31) Sun, H.; Gorelsky, S. I.; Stuart, D. R.; Campeau, L.; Fagnou, K. *J. Org. Chem.* **2010**, *75*, 8180–8189.
- (32) Jover, J.; Fey, N.; Purdie, M.; Lloyd-Jones, G. C.; Harvey, J. N. *J. Mol. Catal. A: Chem.* **2010**, *324*, 39–47.
- (33) Weng, C.; Hong, F. *Dalton Trans.* **2011**, *40*, 6458–6468.
- (34) Braga, A. A. C.; Ujaque, G.; Maseras, F. *Organometallics* **2006**, *25*, 3647–3658.
- (35) Braga, A. A. C.; Morgon, N. H.; Ujaque, G.; Lledós, A.; Maseras, F. *J. Organomet. Chem.* **2006**, *691*, 4459–4466.
- (36) Xue, L.; Lin, Z. *Chem. Soc. Rev.* **2010**, *39*, 1692–1705.
- (37) Goossen, L. J.; Koley, D.; Hermann, H. L.; Thiel, W. *Organometallics* **2006**, *25*, 54–67.
- (38) Goossen, L. J.; Koley, D.; Hermann, H. L.; Thiel, W. *J. Am. Chem. Soc.* **2005**, *127*, 11102–11114.
- (39) Sumimoto, M.; Iwane, N.; Takahama, T.; Sakaki, S. *J. Am. Chem. Soc.* **2004**, *126*, 10457–10471.
- (40) Braga, A. A. C.; Morgon, N. H.; Ujaque, G.; Maseras, F. *J. Am. Chem. Soc.* **2005**, *127*, 9298–9307.
- (41) Gray, B. L.; Wang, X.; Brown, W. C.; Kuai, L.; Schreiber, S. L. *Org. Lett.* **2008**, *10*, 2621–2624.
- (42) Fang, A. G.; Mello, J. V.; Finney, N. S. *Org. Lett.* **2003**, *5*, 967–970.
- (43) Mello, J. V.; Finney, N. S. *Angew. Chem., Int. Ed.* **2001**, *40*, 1536–1538.
- (44) Imhof, W.; Anders, E. *Chem.—Eur. J.* **2004**, *10*, 5717–5729.
- (45) Cheng, H.; Chang, S. *J. Mol. Struct.: THEOCHEM* **2005**, *724*, 209–214.
- (46) Dhoub, A.; Minot, C.; Abderraba, M. *J. Mol. Struct.: THEOCHEM* **2008**, *860*, 161–166.
- (47) Dhoub, A.; Essalah, K.; Tangour, B.; Abderrabba, M. *J. Mol. Struct.: THEOCHEM* **2005**, *715*, 125–131.
- (48) Becke, A. D. *J. Chem. Phys.* **1993**, *98*, 5648–5652.
- (49) Ditchfield, R.; Hehre, W. J.; Pople, J. A. *J. Chem. Phys.* **1971**, *54*, 724–728.
- (50) Lee, C.; Yang, W.; Parr, R. G. *Phys. Rev. B* **1988**, *37*, 785–789.
- (51) Hehre, W. J.; Ditchfield, R.; Pople, J. A. *J. Chem. Phys.* **1972**, *56*, 2257–2261.
- (52) Hariharan, P. C.; Pople, J. A. *Theor. Chim. Acta* **1973**, *28*, 213–222.
- (53) Becke, A. D. *Phys. Rev. A* **1998**, *38*, 3098–3100.
- (54) Burke, K.; Perdew, J. P.; Wang, V. In *Electronic Density Functional Theory: Recent Progress and New Directions*; Dobsin, J. F., Vignale, G., Das, M. P., Eds.; Plenum: New York, 1998.
- (55) Lynch, B. J.; Fast, P. L.; Harris, M.; Truhlar, D. G. *J. Phys. Chem. A* **2000**, *104*, 4811–4815.
- (56) Lynch, B. J.; Truhlar, D. G. *J. Phys. Chem. A* **2001**, *105*, 2936–2941.
- (57) Gonzalez, C.; Schlegel, H. B. *J. Chem. Phys.* **1989**, *90*, 2154–2161.
- (58) Gonzalez, C.; Schlegel, H. B. *J. Phys. Chem.* **1990**, *94*, 5523–5527.
- (59) Cossi, M.; Barone, V.; Mennucci, B.; Tomasi, J. *Chem. Phys. Lett.* **1998**, *286*, 253–260.
- (60) Bader, R. F. W. *Atoms in Molecules. A Quantum Theory*; Clarendon Press: Oxford, 1990. For computer programs, see: Biegler-König, F. W.; Schönbohm, AIM2000. The program can be downloaded at <http://www.aim2000.de/>.
- (61) Blaudéau, J. P.; McGrath, M. P.; Curtiss, L. A.; Radom, L. *J. Chem. Phys.* **1997**, *107*, 5016–5021.
- (62) Francl, M. M.; Pietro, W. J.; Hehre, W. J.; Binkley, J. S.; DeFrees, D. J.; Pople, J. A.; Gordon, M. S. *J. Chem. Phys.* **1982**, *77*, 3654–3665.
- (63) Yoshizawa, K. *Coord. Chem. Rev.* **2002**, *226*, 251–259.
- (64) Frisch, M. J.; Trucks, G. W.; Schlegel, H. B.; Scuseria, G. E.; Robb, M. A.; Cheeseman, J. R.; Montgomery, J. A., Jr.; Vreven, T.; Kudin, K. N.; Burant, J. C.; Millam, J. M.; Iyengar, S. S.; Tomasi, J.; Barone, V.; Mennucci, B.; Cossi, M.; Scalmani, G.; Rega, N.; Petersson, G. A.; Nakatsuji, H.; Hada, M.; Ehara, M.; Toyota, K.; Fukuda, R.; Hasegawa, J.; Ishida, M.; Nakajima, T.; Honda, Y.; Kitao, O.; Nakai, H.; Klene, M.; Li, X.; Knox, J. E.; Hratchian, H. P.; Cross, J. B.; Bakken, V.; Adamo, C.; Jaramillo, J.; Gomperts, R.; Stratmann, R. E.; Yazyev, O.; Austin, A. J.; Cammi, R.; Pomelli, C.; Ochterski, J. W.; Ayala, P. Y.; Morokuma, K.; Voth, G. A.; Salvador, P.; Dannenberg, J. J.; Zakrzewski, V. G.; Dapprich, S.; Daniels, A. D.; Strain, M. C.; Farkas, O.; Malick, D. K.; Rabuck, A. D.; Raghavachari, K.; Foresman, J. B.; Ortiz, J. V.; Cui, Q.; Baboul, A. G.; Clifford, S.; Cioslowski, J.; Stefanov, B. B.; Liu, G.; Liashenko, A.; Piskorz, P.; Komaromi, I.; Martin, R. L.; Fox, D. J.; Keith, T.; Al-Laham, M. A.; Peng, C. Y.; Nanayakkara, A.; Challacombe, M.; Gill, P. M. W.; Johnson, B.; Chen, W.; Wong, M. W.; Gonzalez, C.; Pople, J. A. *Gaussian 03, B05*; Gaussian, Inc.: Wallingford, CT, 2003.
- (65) Shiot, Y.; Suzuki, K.; Yoshizawa, K. *Organometallics* **2005**, *24*, 3532–3538.
- (66) Miyaura, N.; Suzuki, A. *Chem. Rev.* **1995**, *95*, 2457–2483.
- (67) Stille, J. K.; Lau, K. S. Y. *Acc. Chem. Res.* **1977**, *10*, 434–442.
- (68) Snelders, D. J. M.; Koten, G. v.; Gebbink, R. J. M. K. *J. Am. Chem. Soc.* **2009**, *131*, 11407–11416.
- (69) Cargill, M. R.; Sandford, G.; Tadeusiak, A. J.; Yufit, D. S.; Howard, J. A. K.; Kilickiran, P.; Nelles, G. *J. Org. Chem.* **2010**, *75*, 5860–5866.
- (70) García-Cuadrado, D.; Mendoza, P.; de; Braga, A. A. C.; Maseras, F.; Echavarren, A. M. *J. Am. Chem. Soc.* **2007**, *129*, 6880–6886.
- (71) García-Cuadrado, D.; Braga, A. A. C.; Maseras, F.; Echavarren, A. M. *J. Am. Chem. Soc.* **2006**, *128*, 1066–1067.
- (72) Xia, J.; You, S. *Organometallics* **2007**, *26*, 4869–4871.
- (73) Campeau, L.; Parisien, M.; Jean, A.; Fagnou, K. *J. Am. Chem. Soc.* **2006**, *128*, 581–590.
- (74) von Schenck, H.; Åkermarck, B.; Svensson, M. *Organometallics* **2002**, *21*, 2248–2253.
- (75) Drewes, S. E.; Freese, S. D.; Emslie, N. D.; Roos, G. H. P. *Synth. Commun.* **1988**, *18*, 1565–1668.
- (76) Iga, H.; Isozaki, T.; Suzuki, T.; Ichimura, T. *J. Phys. Chem. A* **2007**, *111*, 5981–5987.
- (77) Wilson, S. R.; Perez, J.; Pasternak, A. *J. Am. Chem. Soc.* **1993**, *115*, 1994–1997.
- (78) Aliprantis, A. O.; Canary, J. W. *J. Am. Chem. Soc.* **1994**, *116*, 6985–6986.
- (79) Masllorens, J.; González, I.; Roglans, A. *Eur. J. Org. Chem.* **2007**, 158–166.
- (80) Aramendia, M. A.; Lafont, F. *J. Org. Chem.* **1999**, *64*, 3592–3594.